Received: 9 September 2020 | Revised: 30 October 2020 | Accepted: 4 November 2020

DOI: 10.1111/jnc.15239

ORIGINAL ARTICLE

Journal of Neurochemistry JNC The Official Journal of the International Society for Neurochemistry WILEY

Variability of mitochondrial energy balance across brain regions

XinPing Cheng[1,2] | Andrey Y. Vinokurov[3] | Evgeniy A. Zherebtsov[3,4] | Olga A. Stelmashchuk[3] | Plamena R. Angelova[1] | Noemi Esteras[1] | Andrey Y. Abramov[1,3]

[1]Department of Clinical and Movement Neurosciences, UCL Queen Square Institute of Neurology, London, UK

[2]CAS Key Laboratory of Brain Function and Disease, School of Life Sciences, University of Science and Technology of China, Hefei, China

[3]Cell Physiology and Pathology Laboratory, Orel State University, Orel, Russia

[4]Optoelectronics and Measurement Techniques Laboratory, University of Oulu, Oulu, Finland

Correspondence
Andrey Y. Abramov, Department of Clinical and Movement Neurosciences, UCL Queen Square Institute of Neurology, Queen Square, London, WC1N 3BG, UK.
Email: a.abramov@ucl.ac.uk

Funding information
Russian Federation Government, Grant/Award Number: 075-15-2019-1877; Academy of Finland, Grant/Award Number: 318281

Abstract

Brain is not homogenous and neurons from various brain regions are known to have different vulnerabilities to mitochondrial mutations and mitochondrial toxins. However, it is not clear if this vulnerability is connected to different energy metabolism in specific brain regions. Here, using live-cell imaging, we compared mitochondrial membrane potential and nicotinamide adenine dinucleotide (NADH) redox balance in acute rat brain slices in different brain regions and further detailed the mitochondrial metabolism in primary neurons and astrocytes from rat cortex, midbrain and cerebellum. We have found that mitochondrial membrane potential is higher in brain slices from the hippocampus and brain stem. In primary co-cultures, mitochondrial membrane potential in astrocytes was lower than in neurons, whereas in midbrain cells it was higher than in cortex and cerebellum. The rate of NADH production and mitochondrial NADH pool were highest in acute slices from midbrain and midbrain primary neurons and astrocytes. Although the level of adenosine tri phosphate (ATP) was similar among primary neurons and astrocytes from cortex, midbrain and cerebellum, the rate of ATP consumption was highest in midbrain cells that lead to faster neuronal and astrocytic collapse in response to inhibitors of ATP production. Thus, midbrain neurons and astrocytes have a higher metabolic rate and ATP consumption that makes them more vulnerable to energy deprivation.

KEYWORDS

astrocyte, ATP, brain regions, mitochondria, mitochondrial membrane potential, neuron

1 | INTRODUCTION

Despite the fact that the brain is relatively small compared to the rest of the body (1%–1.5%), is one of the most energy-consuming organs and utilizes more oxygen and glucose than any other tissue. The major energy demands of the brain are because of neuronal signaling (~70% is used for calcium signalling, action and resting potentials, glutamate cycling) and the remaining 30% of the energy expenses is associated with non-signaling activities (de novo synthesis of proteins, phospholipids, oligonucleotide turnover, axonal transport, actin cytoskeleton remodelling, etc.) (Dienel, 2019). Importantly, the rate of information processing in the brain is also limited by efficient energy production (Attwell & Laughlin, 2001; Harris et al., 2012). Because of the tight equilibrium between energy production and consumption, the brain is extremely vulnerable to any alterations of this balance, as occurs for example in an ischemic condition.

In the brain, energy in the form of adenosine tri phosphate (ATP) is mainly produced by oxidative phosphorylation in the

Abbreviations: ATP, adenosine tri phosphate; FCCP, carbonyl cyanide-p-trifluoromethoxyphenylhydrazone; HBSS, Hanks' Balanced Salt solution; IAA, iodoacetic acid; NADH, nicotinamide adenine dinucleotide; NADPH, nicotinamide adenine dinucleotide phosphate; Rh123, rhodamine 123; TCA, tricarboxylic acid cycle; TMRM, tetramethylrhodamine; ΔΨm, mitochondrial membrane potential.

Cheng and Vinokurov are joint first authors.

mitochondria, however, to a lesser degree ATP is also produced by glycolysis. Because of anatomical specificity (astrocytes have closer access to the blood vessels), the energy balance in neurons is mostly relying on astrocytic support. Considering this, neurons and astrocytes have a distinctive energy metabolism. Additionally, because of differences in electrophysiological activity and de novo synthesis of proteins, phospholipids, etc., the rate of energy consumption in these cells should also be different.

Neurological conditions that lead to neuronal cell death, such as ischaemia (stroke) or epilepsy, despite the complexity of their aethiopathological mechanism, are high-energy demanding processes (Abramov & Duchen, 2010; Kovac et al., 2012; Tambasco et al., 2018). All neurodegenerative disorders have shown to have energy metabolism or/and mitochondrial dysfunction involved in the mechanism of development of pathology (Abramov & Angelova, 2019). It should be also noted that mitochondrial toxins (rotenone and MPP+) induce neuronal loss in specific brain regions initiating Parkinson's disease (Hartley et al., 1994; Singer & Ramsay, 1990), or changes in frataxin leading to Friederich's Ataxia (Abeti et al., 2016; Lodi et al., 2002). However, the reason for the specific vulnerability of neurons in particular brain regions to mitochondrial toxins or mitochondrial dysfunction is not clear. One of the possible explanations could be the distinctive rate of energy production or consumption in these areas. A number of approaches have been used for the detection of different parameters of energy metabolism including ATP levels and the rate of glucose metabolism (Kleinridders et al., 2018). Despite that, the mitochondrial membrane potential ($\Delta\Psi m$) should have some defined? range values to act as a proton-motive force for ATP production, the level of $\Delta\Psi m$ can generally vary in cells and this can have effect on some signalling processes, for example, Ca^{2+} uptake and reactive oxygen species production (Esteras et al., 2017; Yao et al., 2011). However, it is not clear how $\Delta\Psi m$ and mitochondrial metabolism vary between neurons and astrocytes in different brain regions, and how fast these cells consume ATP.

Here, we studied differences in $\Delta\Psi m$ and nicotinamide adenine dinucleotide (NADH) redox index in acute live brain slices from different brain regions. Using primary co-cultures of neurons and astrocytes from cortex, midbrain and cerebellum we studied the differences in the $\Delta\Psi m$, NADH redox balance, ATP level and the rate of ATP consumption between neurons and astrocytes from these brain regions.

2 | MATERIALS AND METHODS

The study was not pre-registered. No blinding was performed.

2.1 | Acute brain slices

All animal work for isolation and preparation of brain slices was approved by the Institutional ethical committee of Orel State University (Minutes No. 18 dated 21.02.2020) in compliance with Russian Federation legislation. The rats were group-housed and maintained on a 12-hr light cycle (lights on 07:00) and had ad libitum access to water and food. The experiments were conducted on male Wistar rats (12 for all preparations) at 12 weeks of age (250–300 g). The animals were killed by cervical dislocation. After isolation, the rat brain was placed in chilled Hanks' Balanced Salt solution (HBSS). Horizontal sections of different brain regions (hippocampus, cortex, cerebellum, brain stem) with a thickness of 500 μm were cut—according to the standard procedures (Angelova & Muller, 2006; Novikova et al., 2020) and stored prior to experiments for at least 1 hr/37°C.

2.2 | NADH and Rh123 fluorescence measurements in acute brain slices

To measure the mitochondrial membrane potential with rhodamine 123 (Rh123) or the endogenous content of NADH in acute brain slices, the setup was assembled in two versions: with a BDL-SMN-375 laser source (Becker & Hickl) for excitation of NADH fluorescence at a wavelength of 375 nm or LED M455F1 (Thorlabs Inc., USA) for excitation of Rh123 fluorescence at a wavelength of 490 nm. In this system, the excitation radiation through the optical fiber passes through the collimator and the band-pass filter (when using LED M455F1), and then, through the beam splitting filter plate and the lens is directed to the studied area. Emitted fluorescence light was reflected through a 416 nm (in the configuration for NADH measurements) or 490 nm long-pass filters (in the configuration for Rh123) to a highly sensitive DCC 3260C cooling CCD camera (Thorlabs et al., USA). The field of view of the camera on the sample is a rectangular section with an area of about 1 mm^2. The fluorescence imaging channel reflected from the light source through filters and a highly sensitive DCC 3260C cooling CCD camera is recorded (Thorlabs et al., USA). Brain slices were loaded with 1 μM Rhodamine123 (Rh123) (Molecular Probes; catalog # R22420) for 20 min before experiments. Rh123 has a slower permeability for plasmalemmal membrane compared to other cationic indicators that makes it a better candidate to be used in de-quench mode which is less dependent on the changes in the focal plane.

2.3 | Primary co-cultures of neurons and astrocytes

Mixed cultures of cortical, midbrain and cerebellar granule neurones and glial cells were prepared as described previously (Maiolino et al., 2019) with modifications, from Sprague–Dawley rat pups (22 either sex for all cell preparations) 2–4 days post-partum (UCL breeding colony). Pups were killed by cervical dislocation. Experimental procedures were performed in compliance with the United Kingdom Animals (Scientific Procedures) Act of 1986 and with the European directive 2010/63/EU. Cerebellum, cortex and midbrain were isolated from 2 pups and moved into ice-cold

HBSS (Ca^{2+}, Mg^{2+}-free; Invitrogen, Catalog #14175046). The tissue was minced and trypsinized (0.1% for 15 min at 37°C), triturated and plated on poly-D-lysine-coated coverslips and cultured in Neurobasal A medium (Gibco-Invitrogen, catalog # 21103049) supplemented with B-27 (Gibco-Invitrogen, Catalog # 17504044) and L-glutamine. Cultures were maintained at 37°C in a humidified atmosphere of 5% CO_2 and 95% air, fed twice a week and maintained for a minimum of 12 days before experimental use to ensure the expression of glutamate and other receptors. Neurons were easily distinguishable from glia: they appeared phase bright, had smooth rounded somata and distinct processes, and lay just above the focal plane of the glial layer. Cells were used after days 12–15.

2.4 | Live cell imaging

Measurement of cellular free magnesium using the Mg^{2+}-sensitive fluorescent probe Mag-Fura-2 can be used as an indirect indicator of ATP consumption/production (Ludtmann et al., 2016). Mag-Fura-2 AM (Invitrogen, Catalog number # M1291) dye was added with 0.005% pluronic acid for 30 min in HBSS solution (Invitrogen, catalog # 14025092). The energy capacity of the cell was assessed as the time between the application of inhibitors and the time of cell lysis. Fluorescence measurements were obtained on an epifluorescence inverted microscope equipped with a 20× fluorite objective. $[Mg^{2+}]_c$ was monitored in single cells using excitation light provided by a Xenon arc lamp, the beam passing monochromator at 340 and 380 nm (Cairn Research). Emitted fluorescence light was reflected through a 515 nm long-pass filter to a cooled CCD camera (Retiga; QImaging) and digitized to 12-bit resolution. All imaging data were collected and analysed using software from Andor.

NADH autofluorescence was measured using an epifluorescence inverted microscope equipped with a ×20 fluorite objective. Excitation light at a wavelength of 360nm was provided by a Xenon arc lamp, the beam passing through a monochromator (Cairn Research). Emitted fluorescence light was reflected through a 455 nm long-pass filter to a cooled CCD camera (Retiga; QImaging) and digitized to 12 bit resolution (Al-Menhali et al., 2020). Imaging data were collected and analysed using Andor iQ3 imaging software.

Confocal images were obtained using Zeiss 710 CLSM microscope equipped with a META detection system and a 40× oil immersion objective. Mitochondrial membrane potential was identified using the potential sensitive indicator tetramethylrhodamine (TMRM) (Invitrogen catalog number # T668). Cells were loaded for 40 min at room temperature (25°C) and superfused with 25 nM TMRM, excited at 565 nm and imaged with a 580 nm emission filter as previously described (Angelova et al., 2018; Bartolome et al., 2017). Measurements of TMRM fluorescence in neurons and astrocytes were determined across z-tacks. Illumination intensity was kept to a minimum (at 0.1%–0.2% of the max laser output) to avoid phototoxicity and the pinhole set to give an optical slice of ~2 μm.

To determine the ATP levels, primary co-cultures were transfected with a mitochondrially targeted ATP probe (AT1.03) generated by Imamura et al. (Imamura et al., 2009), using Effectene (Qiagen) according to the manufacturer's instructions. The FRET was quantified by the 527:475 nm ratio after an excitation with 405 nm and a filtered at 515–580 nm (Ludtmann et al., 2014).

2.5 | Statistical analysis

Results are expressed as means ± *SEM* (standard error of the mean); one-way ANOVA with post hoc Tukey's HSD correction for multiple comparisons and Student's *t* test were used, where appropriate. Statistical analysis was performed using Origin 2019 (Microcal Software Inc.) software. Differences were considered to be significantly different if $p < .05$. No exclusion criteria were pre-determined. No sample size calculation was performed, the number of rats was taken as a number of cell preparations or brain slices preparation. No test for outliers was conducted. Data were not assessed for normality.

3 | RESULTS

Measurements of mitochondrial membrane potential in acute rat brain slices from different regions with Rhodamine123 showed that ΔΨm is not equal between them (Figure 1a). To avoid any misinterpretations of the results, 1μM carbonyl cyanide-p-trifluoromethoxyphenylhydrazone (FCCP) was added at the end of each experiment to induce depolarization that led to the redistribution of the Rh123 from mitochondria to the cytosol and was registered as an increase in Rh123 fluorescence. When the indicator diffused out through the plasmalemmal membrane t could be seen from the slow decrease in Rh123 fluorescence after the FCCP-induced peak (Figure 1b,c). The highest values of ΔΨm were observed in hippocampal slices (155 ± 7% of cortical ΔΨm; $N = 7$ rats, $n = 14$ slices; Figure 1a,b) and in slices from brain stem (195 ± 11%; $N = 7$ rats, $n = 14$ slices; Figure 1a). Mitochondrial membrane potential in cells of midbrain slices was also higher compared to the cortex (127 ± 7%; $N = 7$ rats, $n = 14$ slices; Figure 1a), whereas ΔΨm in cerebellar slices was similar to cortices (Figure 1a,c).

Mitochondrial membrane potential might be different because of a number of factors including activity of the electron transport chain of the mitochondria, the level of uncoupling proteins, or the mechanism of maintenance of ΔΨm. To find out what causes the differences in the activity of mitochondrial electron transport chain in different brain regions, we measured NADH level in various parts of acute brain slices.

3.1 | NADH redox state in acute brain slices from different regions

NADH is a major donor of electrons in mitochondrial complex I and measurements of NADH autofluorescence can give information about the activity of mitochondrial respiration in live cells. To

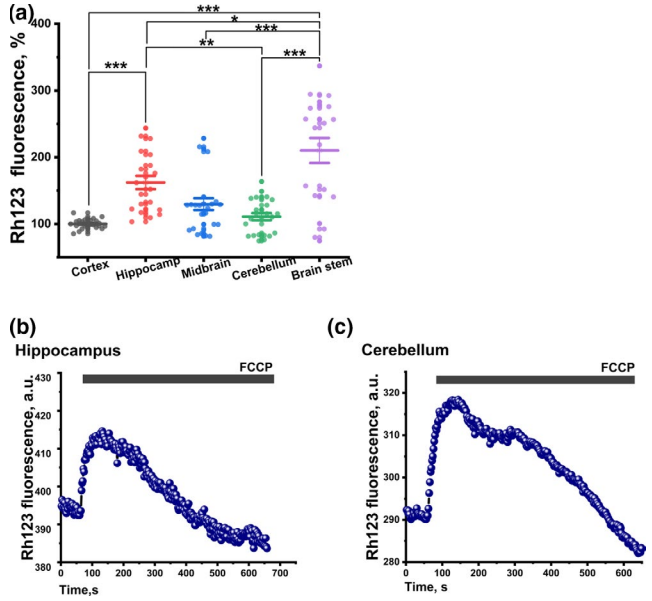

FIGURE 1 Mitochondrial membrane potential in acute slices from different brain regions. Mitochondrial membrane potential ($\Delta\Psi m$) was measured using Rhodamine123 as a fluorescent indicator. (a) $\Delta\Psi m$ in acute slices of different brain regions. For each brain region $N = 7$ rats, $n = 14$ slices. Rhodamine123 fluorescence in cortical slices was taken as 100%. (b, c) Effect of 1μM carbonyl cyanide-p-trifluoromethoxyphenylhydrazone (FCCP) on Rhodamine123 fluorescence in hippocampal and cerebellar slices. The error bars depict mean ± *SEM*, statistical significance was calculated using one-way ANOVA with post hoc Tukey's HSD correction for multiple comparisons. $^{*}p < .05$; $^{**}p < .01$; $^{***}p < .001$

distinguish mitochondrial NADH fluorescence from nicotinamide adenine dinucleotide phosphate (NADPH) signal and non-mitochondrial NADH, we maximized respiration in brain slices by adding 1μM FCCP (which minimizes mitochondrial NADH level—0%) followed by inhibition of respiration by 1 mM NaCN, that blocks consumption of NADH and maximally increases NADH level in mitochondria (Figure 2a,b). The difference in NADH between minimal and maximal values could be taken as a mitochondrial NADH pool. Interestingly, mitochondrial NADH pool in midbrain cells was significantly higher compared to mitochondrial NADH level in cells from cortical, hippocampal, brain stem and cerebellar slices (Figure 2b–g).

NADH redox level reflects the balance between NADH production and NADH consumption in mitochondria. The lowest level we observed in hippocampal (41 ± 3%; $N = 5$ rats, $n = 15$ slices) and cerebellar (38 ± 3%, $N = 5$ rats, $n = 15$ slices) slices suggests higher respiratory activity in these brain regions. The highest NADH redox level was observed in midbrain (62 ± 5%, $N = 5$ rats, $n = 14$ slices) and brain stem (58 ± 5%, $N = 5$ rats, $n = 14$) slices (Figure 2b–f,h). Inhibition of the mitochondrial respiration with NaCN completely blocks the consumption of NADH in complex I and the rate of rise of NADH could be accepted as the rate of NADH production in tricarboxylic acid cycle (Krebs cycle) (Figure 2b for explanation—see also Figure 2b–f,i). The rate of NADH production was different in slices from various brain regions with the highest values in midbrain and

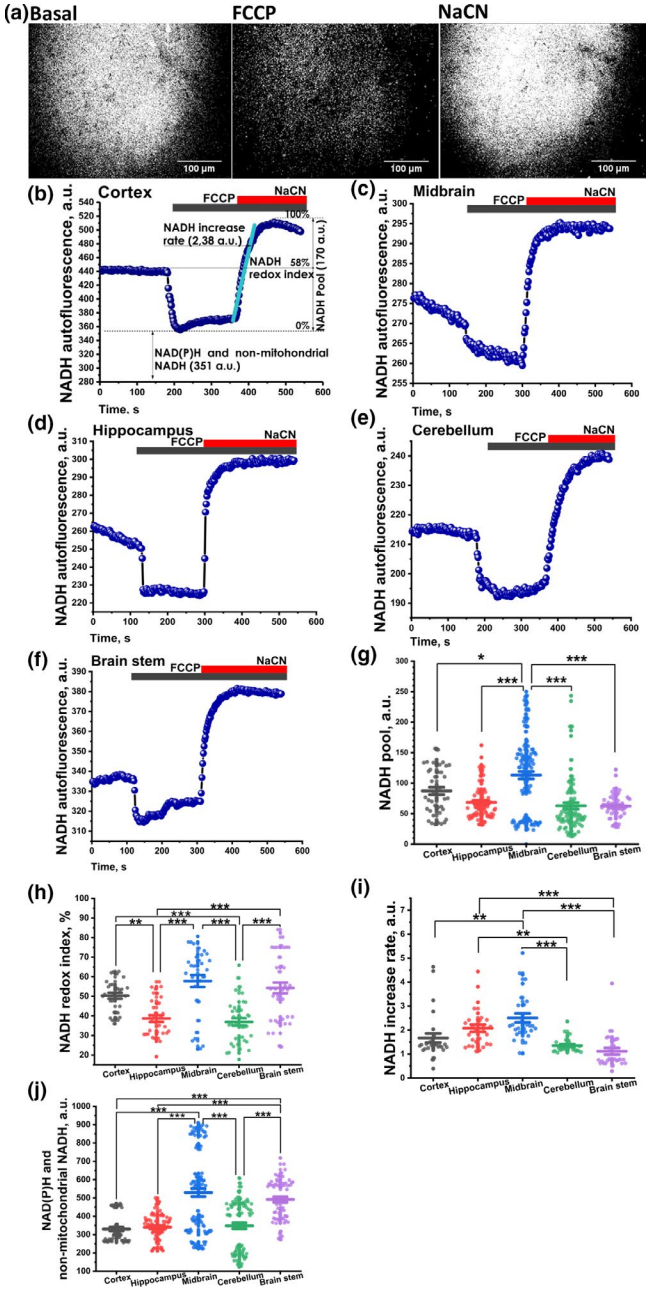

FIGURE 2 Difference in mitochondrial nicotinamide adenine dinucleotide (NADH) level and redox state in acute slices from brain regions. (a) Representative images of NADH autofluorescence in cortical acute slices before and after application of 1μM carbonyl cyanide-p-trifluoromethoxyphenylhydrazone (FCCP) and 1mM NaCN. Representative traces of NADH autofluorescence from acute slices from cortex (b), midbrain (c), hippocampus (d), cerebellum (e) and brain stem (f). Experiment in (a) is taken as example how different NADH parameters were calculated including mitochondrial NADH pool (g), NADH redox state (h), rate of NADH increase after 1mM NaCN application (i) and non-mitochondrial NADH and nicotinamide adenine dinucleotide phosphate (NADPH) pool (j) in acute slices. For each brain region measurements—$N = 5$ rats, $n = 14$ slices. The error bars depict mean ± *SEM*, statistical significance was calculated using ANOVA with the Tukey post hoc test. $^{*}p < .05$; $^{**}p < .01$; $^{***}p < .001$

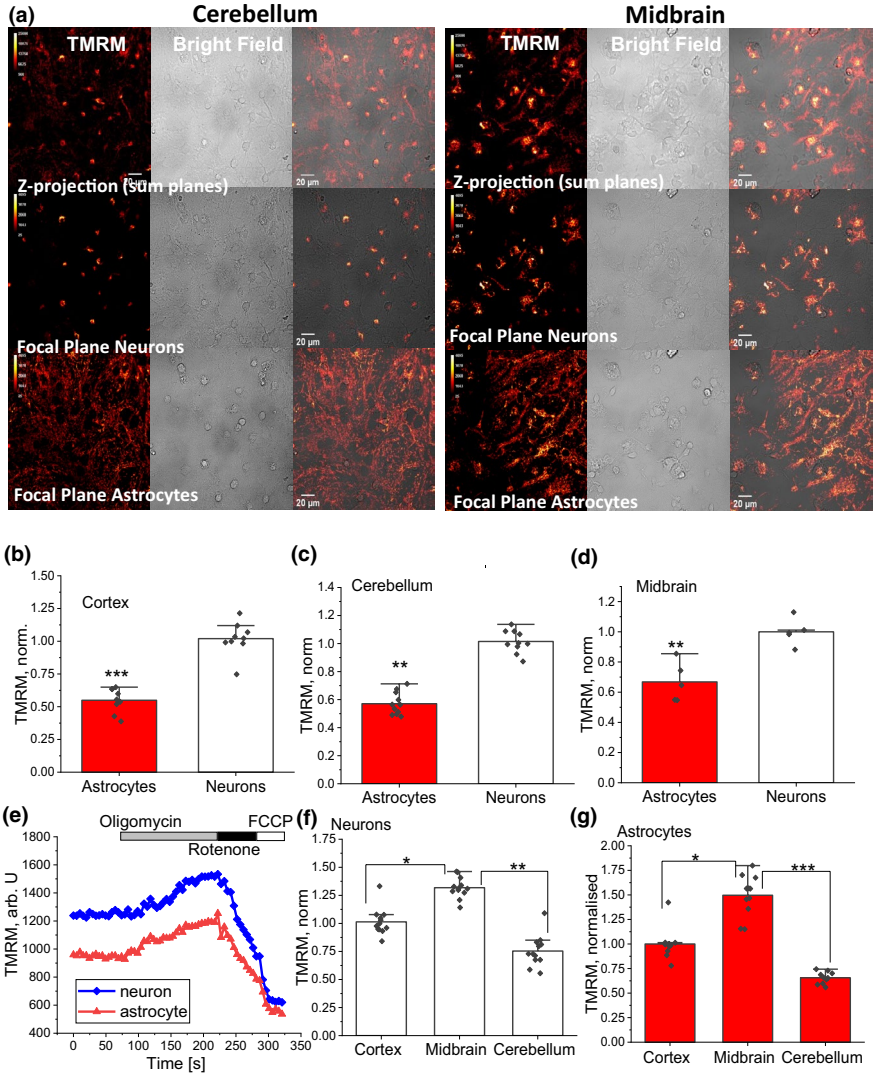

FIGURE 3 Difference in mitochondrial membrane potential (ΔΨm) between primary neurons and astrocytes isolated from cortex, midbrain and cerebellum. (a) Mitochondrial membrane potential in primary co-cultures was assessed using different Z-projections for separation of the tetramethylrhodamine (TMRM) signal from neurons and astrocytes and identification of the maximal fluorescence from mitochondria of live cells. Mitochondrial membrane potential is higher in neurons than in astrocytes in primary cortical (b, $N = 5$ cell culture preparations), cerebellar (c; $N = 7$ cell culture preparations) and midbrain (d; $N = 7$ cell culture preparations). TMRM was normalized as 100% to neurons. (e) Measurement of TMRM fluorescence in response to applications of 2µg/ml oligomycin, 1 µM rotenone and 1 µM carbonyl cyanide-p-trifluoromethoxyphenylhydrazone (FCCP) to midbrain neurons and astrocytes. Difference in ΔΨm between neurons (f) and astrocytes (g) from primary co-cultures of cortex, midbrain and cerebellum. ΔΨm in astrocytes and neurons from cortical cultures were taken as 100%. $^{*}p < .05$; $^{**}p < .01$; $^{***}p < .001$

hippocampus (Figure 2i). Considering that the highest rate of NADH production is found in the mitochondria of cells from midbrain slices (Figure 2i), the elevated NADH redox level in this region could be explained by the higher production rate, whereas in brain stem it more likely because of a lower respiratory activity.

Interestingly, the level of NADPH and non-mitochondrial NADH (which was measured as the autofluorescence insensitive to FCCP and NaCN) was also highest in the midbrain area (Figure 2j) and the brain stem. Non-mitochondrial NADH/NADPH levels in the brain stem and the cerebellum were higher compared to the cortical or the hippocampal areas (Figure 2j).

Broad distribution of the signal of ΔΨm and NADH parameters in brain slices can be explained by the short lifetime of ex vivo models and assessment of bioenergetics in different brain regions could not be complete without understanding the interaction between neurons and astrocytes in primary co-cultures. Considering this, we produced primary co-cultures of neurons and astrocytes from the most vulnerable regions to ischaemia and mitochondrial toxins—cortex, midbrain and cerebellum and compared the major bioenergetic characteristics between cells and brain regions.

3.2 | ΔΨm is higher in neurons compared to astrocytes in the co-cultures

In primary co-cultures neurons and astrocytes are distributed in different layers and very often are pooled in measurements of mitochondrial membrane potential. Using Z-stacks we were able to separate the signals and compared ΔΨm in neurons and astrocytes (Figure 3a). In all studied primary co-cultures—cortical, midbrain and cerebellar, mitochondrial membrane potential in neurons was significantly higher than in astrocytes. Thus, the maximal difference in ΔΨm between cell types was observed in cortical co-cultures where the level of TMRM fluorescence in astrocytes was significantly smaller (Figure 3b; 51 ± 4% of neuronal, $N = 5$ experiments, $n = 155$ cells; $p < .001$). In cerebellar and midbrain co-cultures ΔΨm of astrocytes was also low—58 ± 5% and 67 ± 7% of neighbouring neurons respectively (Figure 3c,d; $N = 7$ experiments).

Despite the difference in the ΔΨm between neurons and astrocytes, the mechanism of maintenance of mitochondrial membrane potential is similar for both types of cells. Thus, application of the inhibitor of F_0-F_1-ATP synthase oligomycin (2 µg/ml) to midbrain co-culture of neurons

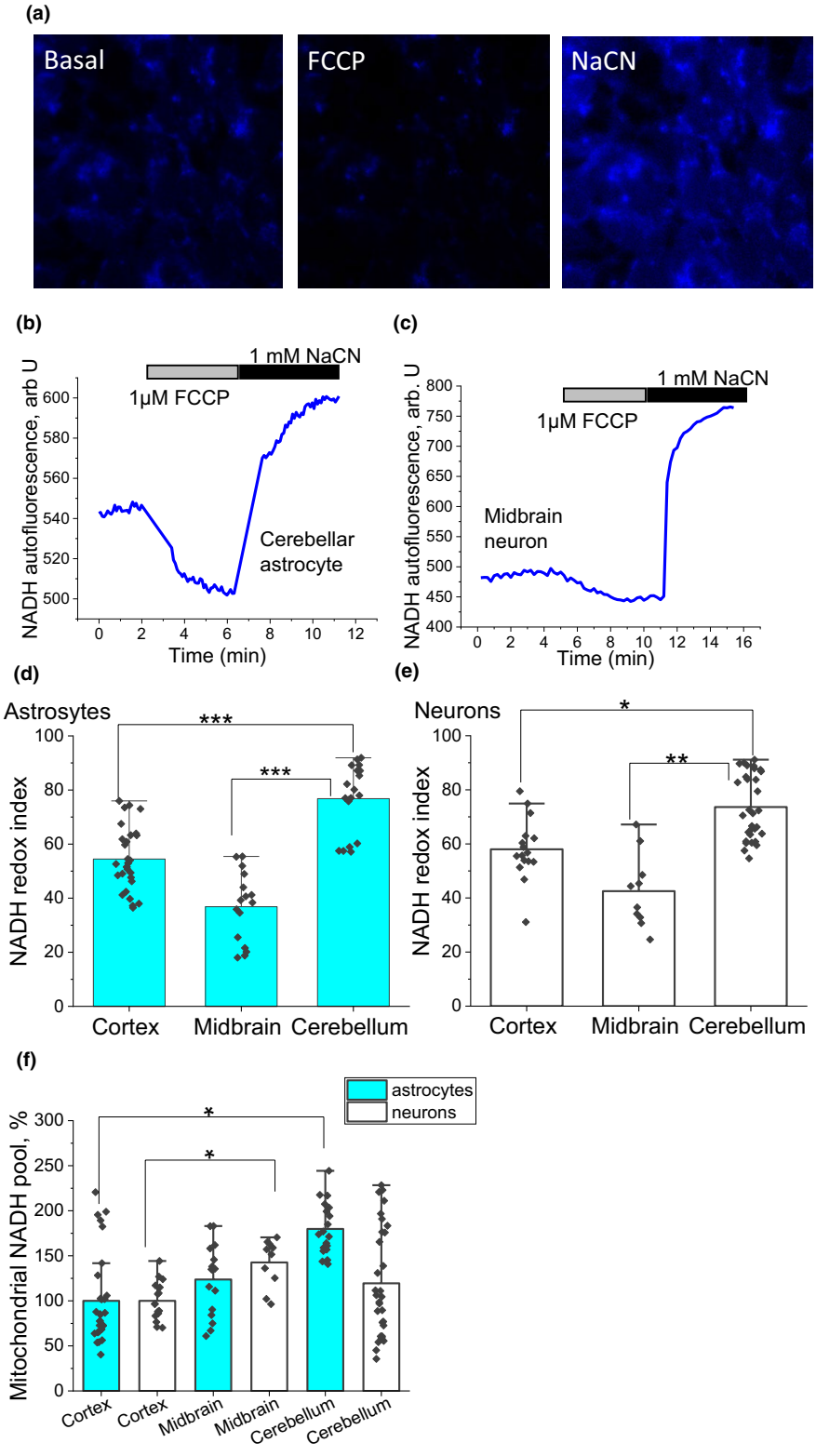

FIGURE 4 Comparison of mitochondrial nicotinamide adenine dinucleotide (NADH) redox level and NADH pools in primary neurons and astrocytes isolated from cortex, midbrain and cerebellum. Representative images (a) and traces of NADH autofluorescence in response to 1 μM carbonyl cyanide-p-trifluoromethoxyphenylhydrazone (FCCP) and 1 mM NaCN in cerebellar astrocyte (b) and midbrain neuron (c). Mitochondrial NADH redox indexes are calculated for astrocytes (d) and neurons (e). (f) Difference in mitochondrial NADH pool between neurons and astrocytes from primary co-cultures of cortex, midbrain and cerebellum. For experiments on primary neurons and astrocytes from each regions $N = 5$ cell culture preparations. $^{*}p < .05$; $^{**}p < .01$; $^{***}p < .001$

and astrocytes induced an increase in TMRM fluorescence by ~20% in both type of cells, that strongly suggests that ΔΨm is not maintained by hydrolysis of ATP in the F_0-F_1-ATPase ($N = 4$ experiments; Figure 3e). Subsequent application of the inhibitor of complex I rotenone (1 μM) led to profound mitochondrial depolarization with a relatively small effect of the uncoupler FCCP (1 μM) confirming that ΔΨm in neurons and astrocytes is maintained by the electron transport chain (Figure 3e).

3.3 | ΔΨm in primary neurons and astrocytes in midbrain is higher than in cortical or cerebellar cells

Midbrain neurons had the highest mitochondrial membrane potential (124 ± 8% of cortical neurons, Figure 3f), whereas primary neurons from cerebellum had the lowest one (78 ± 8% of cortical; Figure 3f). A similar difference between cells from the three

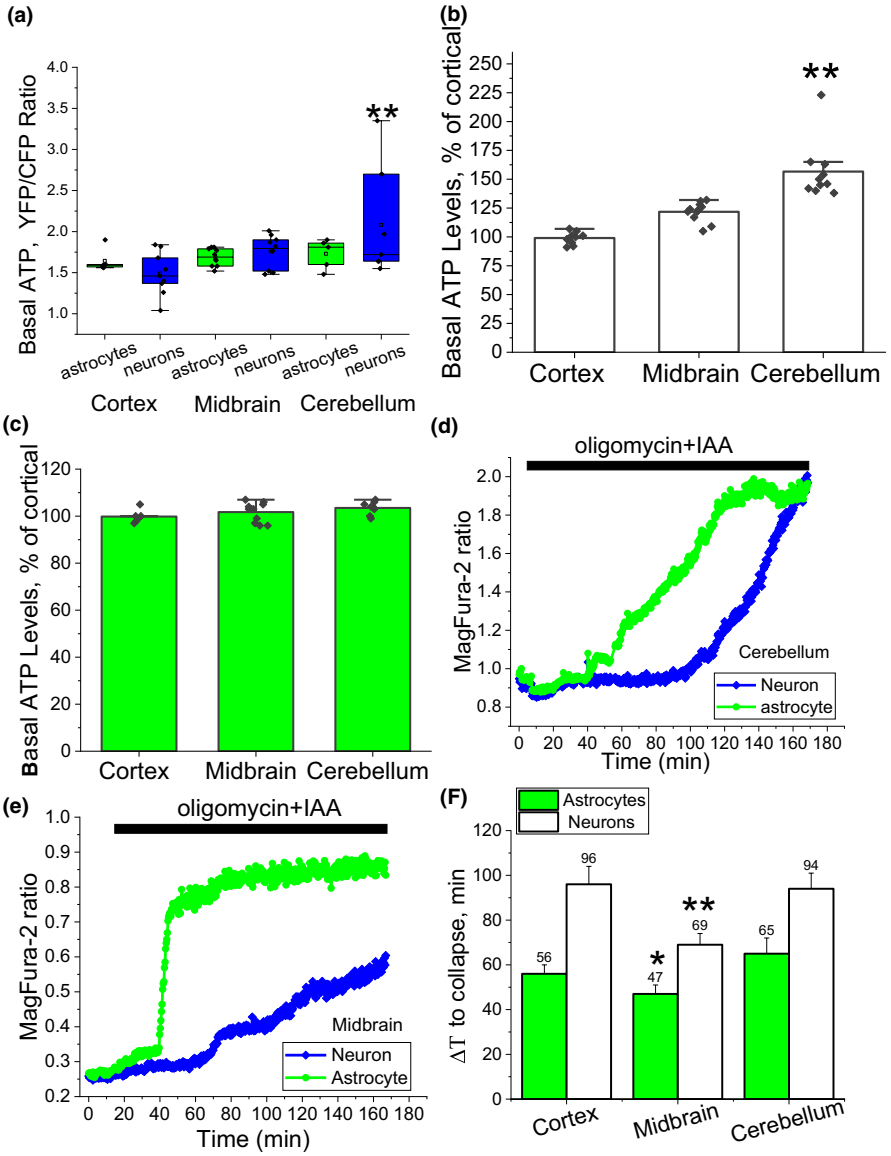

FIGURE 5 Adenosine tri phosphate (ATP) levels and rate of ATP consumption in primary neurons and astrocytes isolated from cortex, midbrain and cerebellum. (a–c) Basal ATP levels were estimated in neurons and astrocytes after transfection of the genetically encoded, mitochondrially targeted probe AT1.03 as described in Methods. For experiments on primary neurons and astrocytes from each regions $N = 5$ cell culture preparations. (d–f) Rate of ATP consumption was indirectly calculated as the rate of increase in free magnesium that occurs upon ATP-hydrolysis, after blocking ATP production with oligomycin and iodoacetic acid. ATP depletion leads to cell collapse that is detected by a sudden increase in fluorescence. Representative traces of ATP consumption in cerebellum (d) and midbrain cells (e). (f) Time to cell collapse after blocking ATP production in cortical ($N = 5$ cell culture preparations) midbrain ($N = 4$) and cerebellum ($N = 4$ cell preparations) neurons and astrocytes. $^{*}p < .05$; $^{**}p < .01$; $^{***}p < .001$

brain regions was also observed for astrocytes (Figure 3g). Thus, the difference in ΔΨm between midbrain and cortical astrocytes was even higher (141 ± 10% in midbrain, Figure 3e) and lower in cerebellar astrocytes (62 ± 6% of cortical astrocytes, Figure 3g).

3.4 | Mitochondrial NADH level in primary co-cultures

Mitochondrial NADH level and NADH pool in primary co-cultures were assessed in the same way as in experiments with acute brain slices (Figure 2), but in these experiments, we were able to distinguish autofluorescence of NADH from neurons and astrocytes (Figure 4a–c).

Despite the dramatic difference in ΔΨm between neurons and astrocytes, NADH redox level, which mostly corresponds to the rate of respiration in these cells, was not significantly different between astrocytes and neurons in co-cultures from cortex, midbrain and cerebellum (Figure 4b–e). Importantly, despite the potential difference in the mechanisms of bioenergetics between these cells, mitochondrial pool was also similar between astrocytes and neurons in cortical, midbrain and cerebellar primary co-cultures that in combination with redox state suggests equal production of NADH in the tricarboxylic acid cycle cycle (Figure 4f). However, redox index in midbrain neurons (52 ± 4, $n = 130$ cells) and astrocytes (48 ± 4, $n = 149$ cells) was significantly lower compared to cells from the cerebellum (75 ± 3, $n = 210$ astrocytes; 71 ± 2, $n = 158$ neurons) or the cortex (55 ± 2, $n = 170$ astrocytes; 58 ± 2, $n = 139$ neurons) (Figure 4c,d) that is in agreement with the results of ΔΨm measurements in these cells from these regions. Interestingly, the NADH pool in primary neurons and astrocytes from the cortex was lower compared to the cerebellum and midbrain (Figure 4e,f).

3.5 | Intracellular ATP level in primary co-cultures of neurons and astrocytes

Intracellular level of ATP was assessed using the mitochondrially targeted FRET probe AT1.03 (Imamura et al., 2009). The basal

level of ATP was different between neurons and astrocytes and this difference was dependent on the brain regions (Figure 5). Thus, cortical astrocytes have a higher $[ATP]_m$ compared to neighbouring neurons (110.3 ± 4.3% of neuronal; Figure 5a). In midbrain astrocytes, the level of ATP was almost similar to neuronal (96 + 1.9%; Figure 5a), whereas in cerebellar co-culture astrocytic $[ATP]_m$ was lower than in neurons (89 ± 4.1%; Figure 5a). Interestingly, the basal ATP level was similar between astrocytes from cortical, midbrain and cerebellum (Figure 5d). Cerebellar neurons in our experiments had the highest ATP level (130% of cortical, $N = 4$; Figure 5e) and in midbrain neurons it was also relatively high—118 ± 4% of cortical.

3.6 | ATP consumption in primary co-cultures

The basal level of ATP is an important characteristic of the cell energy metabolism, but it reflects the balance between ATP production and consumption in resting cells at a certain point. To identify the rate of ATP consumption of neurons and astrocytes from different brain regions, we estimated the levels of cellular free magnesium using the indicator Mag-Fura-2 in the presence of inhibitors of the ATP production.

Mg^{2+} is released from the Mg-ATP complex upon hydrolysis of ATP, and therefore, changes in the fluorescence of Mag-Fura-2 can be used as an indirect probe for ATP consumption (Leyssens et al., 1996). Mag-fura-2 is also a low-affinity Ca^{2+} indicator, and this feature allowed us to detect the cell collapse caused by the inability to maintain the ionic homeostasis upon ATP depletion, which appears as a sudden increase in the Mag-Fura-2 fluorescence because of a massive calcium influx.

Co-application of inhibitors of oxidative phosphorylation (2μg/ml oligomycin) and glycolysis (20 μM iodoacetic acid) blocks the main sources of ATP production, and from that point, cells can only consume the ATP already available in the cells. This allows us to estimate the rate of ATP consumption independently of the production.

Interestingly, although neurons are thought to be more energy-demanding cells compared to astrocytes, inhibition of ATP synthesis led to a faster energy depletion and cell lysis in astrocytes compared to neurons (Figure 5d–f). This effect was observed for cortical, midbrain and cerebellum co-cultures (Figure 5f).

The midbrain neurons from primary co-cultures were the most vulnerable to inhibition of ATP production and showed the shortest time (69 ± 5 min, $N = 4$ experiments, $n = 87$ cells) to energy collapse, compared to cortical (96 ± 8 min, $N = 5$ experiments, $n = 103$ cells) or cerebellar neurons (94 ± 7 min; $N = 4$ experiments, $n = 97$ cells; Figure 5d–f).

4 | DISCUSSION

Although the production of ATP in mitochondria requires a very narrow range of proton motive force and values mitochondrial membrane potential, correspondingly (Mitchell, 1961), here we found that ΔΨm is highly variable across cell types (neurons and astrocytes) and brain regions. Considering the similar levels of ATP in these cells, (Figure 5) we suggest that the difference in ΔΨm is dependent on the rate of metabolism and mechanism of maintenance of mitochondrial membrane potential. Additionally, ΔΨm is important for mitochondrial calcium uptake (Abeti & Abramov, 2015) and the difference between neurons and astrocytes may reflect the high importance of calcium buffering in mitochondria for neurons.

Higher demands of midbrain neurons for ATP availability have been suggested before (Surmeier et al., 2017), and explained by the difference in ATP consumption rates between Na^+/K^+ ATPase and Ca^{2+}-ATPase. In agreement with this, we have found that midbrain neurons consume ATP much faster compared to cortical and cerebellar neurons. Although we have not separated the signal from more specialized neurons (such a dopaminergic, striatal, etc.) because of technical difficulties, the variety of responses of neurons to ATP production inhibition can suggest that some specialized neurons consume ATP faster than other types of neurons. Interestingly, despite the presence of electrical activity of neurons compared to astrocytes (Verkhratsky et al., 2017), astrocytes from different brain areas consumed ATP faster and thus collapsed faster compared to neurons, despite the similar basal level of ATP (Figure 5). This is an interesting observation and could be explained by the supporting function of astrocytes towards neurons and could further elucidate why the astrocyte–neuron interaction is vitally important in the development of pathology of neurological diseases (Angelova & Abramov, 2014).

Basal ATP level is similar for most of the cells except for cerebellar neurons and the rate of ATP consumption is higher in midbrain neurons and astrocytes. Thus, NADH pool in these cells, together with the rate of NADH production were elevated, and were associated with a similar or higher rate of mitochondrial respiration (NADH redox index, Figures 2 and 4). Importantly, this increased rate of respiration and metabolism was not associated with mitochondrial uncoupling because the ΔΨm was also high in primary midbrain neurons and astrocytes. Thus observed higher rate of ATP consumption and higher consumption rate of mitochondrial complex I substrates might potentially explain why this brain region is particularly vulnerable to the action of mitochondrial toxins and pesticides and severe bioenergetic disbalance might contribute to trigger dopaminergic neurodegeneration in Parkinson's disease (Abramov & Angelova, 2019; Betarbet et al., 2000; Schapira et al., 1989).

ACKNOWLEDGEMENTS

This work was supported by the grant of the Russian Federation Government Nr. 075-15-2019-1877. E.Z. acknowledges the support of the Academy of Finland (Grant No. 318281).

All experiments were conducted in compliance with the ARRIVE guidelines.

CONFLICT OF INTEREST

The authors declare that they have no known competing financial interests or personal relationships that could have appeared to influence the work reported in this paper.

ORCID

Andrey Y. Abramov https://orcid.org/0000-0002-7646-7235

REFERENCES

Abeti, R., & Abramov, A. Y. (2015). Mitochondrial Ca(2+) in neurodegenerative disorders. *Pharmacological Research*, *99*, 377–381. https://doi.org/10.1016/j.phrs.2015.05.007

Abeti, R., Parkinson, M. H., Hargreaves, I. P., Angelova, P. R., Sandi, C., Pook, M. A., Giunti, P., & Abramov, A. Y. (2016). Mitochondrial energy imbalance and lipid peroxidation cause cell death in Friedreich's ataxia. *Cell Death & Disease*, *7*, e2237. https://doi.org/10.1038/cddis.2016.111

Abramov, A. Y., & Angelova, P. R. (2019). Mitochondrial dysfunction and energy deprivation in the mechanism of neurodegeneration. *Turkish Journal of Biochemistry*, *44*, 723–729. https://doi.org/10.1515/tjb-2019-0255

Abramov, A. Y., & Duchen, M. R. (2010). Impaired mitochondrial bioenergetics determines glutamate-induced delayed calcium deregulation in neurons. *Biochimica Et Biophysica Acta*, *1800*, 297–304. https://doi.org/10.1016/j.bbagen.2009.08.002

Al-Menhali, A. S., Banu, S., Angelova, P. R., Barcaru, A., Horvatovich, P., Abramov, A. Y., & Jaganjac, M. (2020). Lipid peroxidation is involved in calcium dependent upregulation of mitochondrial metabolism in skeletal muscle. *Biochimica Et Biophysica Acta - General Subjects*, *1864*, 129487. https://doi.org/10.1016/j.bbagen.2019.129487

Angelova, P. R., & Abramov, A. Y. (2014). Interaction of neurons and astrocytes underlies the mechanism of Abeta-induced neurotoxicity. *Biochemical Society Transactions*, *42*, 1286–1290.

Angelova, P. R., Iversen, K. Z., Teschemacher, A. G., Kasparov, S., Gourine, A. V., & Abramov, A. Y. (2018). Signal transduction in astrocytes: Localization and release of inorganic polyphosphate. *Glia*, *66*, 2126–2136. https://doi.org/10.1002/glia.23466

Angelova, P., & Muller, W. (2006). Oxidative modulation of the transient potassium current IA by intracellular arachidonic acid in rat CA1 pyramidal neurons. *European Journal of Neuroscience*, *23*, 2375–2384.

Attwell, D., & Laughlin, S. B. (2001). An energy budget for signaling in the grey matter of the brain. *Journal of Cerebral Blood Flow and Metabolism*, *21*, 1133–1145. https://doi.org/10.1097/00004647-200110000-00001

Bartolome, F., Esteras, N., Martin-Requero, A., Boutoleau-Bretonniere, C., Vercelletto, M., Gabelle, A., Le Ber, I., Honda, T., Dinkova-Kostova, A. T., Hardy, J., Carro, E., & Abramov, A. Y. (2017). Pathogenic p62/SQSTM1 mutations impair energy metabolism through limitation of mitochondrial substrates. *Scientific Reports*, *7*, 1666. https://doi.org/10.1038/s41598-017-01678-4

Betarbet, R., Sherer, T. B., MacKenzie, G., Garcia-Osuna, M., Panov, A. V., & Greenamyre, J. T. (2000). Chronic systemic pesticide exposure reproduces features of Parkinson's disease. *Nature Neuroscience*, *3*, 1301–1306. https://doi.org/10.1038/81834

Dienel, G. A. (2019). Brain glucose metabolism: Integration of energetics with function. *Physiological Reviews*, *99*, 949–1045. https://doi.org/10.1152/physrev.00062.2017

Esteras, N., Rohrer, J. D., Hardy, J., Wray, S., & Abramov, A. Y. (2017). Mitochondrial hyperpolarization in iPSC-derived neurons from patients of FTDP-17 with 10+16 MAPT mutation leads to oxidative stress and neurodegeneration. *Redox Biology*, *12*, 410–422. https://doi.org/10.1016/j.redox.2017.03.008

Harris, J. J., Jolivet, R., & Attwell, D. (2012). Synaptic energy use and supply. *Neuron*, *75*, 762–777. https://doi.org/10.1016/j.neuron.2012.08.019

Hartley, A., Stone, J. M., Heron, C., Cooper, J. M., & Schapira, A. H. (1994). Complex I inhibitors induce dose-dependent apoptosis in PC12 cells: Relevance to Parkinson's disease. *Journal of Neurochemistry*, *63*, 1987–1990. https://doi.org/10.1046/j.1471-4159.1994.63051987.x

Imamura, H., Nhat, K. P., Togawa, H., Saito, K., Iino, R., Kato-Yamada, Y., Nagai, T., & Noji, H. (2009). Visualization of ATP levels inside single living cells with fluorescence resonance energy transfer-based genetically encoded indicators. *Proceedings of the National Academy of Sciences of the United States of America*, *106*, 15651–15656. https://doi.org/10.1073/pnas.0904764106

Kleinridders, A., Ferris, H. A., Reyzer, M. L., Rath, M., Soto, M., Manier, M. L., Spraggins, J., Yang, Z., Stanton, R. C., Caprioli, R. M., & Kahn, C. R. (2018). Regional differences in brain glucose metabolism determined by imaging mass spectrometry. *Molecular Metabolism*, *12*, 113–121. https://doi.org/10.1016/j.molmet.2018.03.013

Kovac, S., Domijan, A. M., Walker, M. C., & Abramov, A. Y. (2012). Prolonged seizure activity impairs mitochondrial bioenergetics and induces cell death. *Journal of Cell Science*, *125*, 1796–1806. https://doi.org/10.1242/jcs.099176

Leyssens, A., Nowicky, A. V., Patterson, L., Crompton, M., & Duchen, M. R. (1996). The relationship between mitochondrial state, ATP hydrolysis, [Mg2+]i and [Ca2+]i studied in isolated rat cardiomyocytes. *Journal of Physiology*, *496*(Pt 1), 111–128. https://doi.org/10.1113/jphysiol.1996.sp021669

Lodi, R., Rajagopalan, B., Bradley, J. L., Taylor, D. J., Crilley, J. G., Hart, P. E., Blamire, A. M., Manners, D., Styles, P., Schapira, A., & Cooper, J. M. (2002). Mitochondrial dysfunction in Friedreich's ataxia: From pathogenesis to treatment perspectives. *Free Radical Research*, *36*, 461–466. https://doi.org/10.1080/10715760290021324

Ludtmann, M. H., Angelova, P. R., Ninkina, N. N., Gandhi, S., Buchman, V. L., & Abramov, A. Y. (2016). Monomeric alpha-synuclein exerts a physiological role on brain ATP synthase. *Journal of Neuroscience*, *36*, 10510–10521. https://doi.org/10.1523/JNEUROSCI.1659-16.2016

Ludtmann, M. H., Angelova, P. R., Zhang, Y., Abramov, A. Y., & Dinkova-Kostova, A. T. (2014). Nrf2 affects the efficiency of mitochondrial fatty acid oxidation. *The Biochemical Journal*, *457*, 415–424. https://doi.org/10.1042/BJ20130863

Maiolino, M., O'Neill, N., Lariccia, V., Amoroso, S., Sylantyev, S., Angelova, P. R., & Abramov, A. Y. (2019). Inorganic polyphosphate regulates AMPA and NMDA receptors and protects against glutamate excitotoxicity via activation of P2Y receptors. *Journal of Neuroscience*, *39*, 6038–6048. https://doi.org/10.1523/JNEUROSCI.0314-19.2019

Mitchell, P. (1961). Coupling of phosphorylation to electron and hydrogen transfer by a chemi-osmotic type of mechanism. *Nature*, *191*, 144–148. https://doi.org/10.1038/191144a0

Novikova, I. N., Manole, A., Zherebtsov, E. A., Stavtsev, D. D., Vukolova, M. N., Dunaev, A. V., Angelova, P. R., & Abramov, A. Y. (2020). Adrenaline induces calcium signal in astrocytes and vasoconstriction via activation of monoamine oxidase. *Free Radical Biology and Medicine*, *159*, 15–22. https://doi.org/10.1016/j.freeradbiomed.2020.07.011

Schapira, A. H., Cooper, J. M., Dexter, D., Jenner, P., Clark, J. B., & Marsden, C. D. (1989). Mitochondrial complex I deficiency in Parkinson's disease. *Lancet*, *1*, 1269. https://doi.org/10.1016/S0140-6736(89)92366-0

Singer, T. P., & Ramsay, R. R. (1990). Mechanism of the neurotoxicity of MPTP. An update. *FEBS Letters*, *274*, 1–8.

Surmeier, D. J., Obeso, J. A., & Halliday, G. M. (2017). Selective neuronal vulnerability in Parkinson disease. *Nature Reviews Neuroscience*, *18*, 101–113. https://doi.org/10.1038/nrn.2016.178

Tambasco, N., Romoli, M., & Calabresi, P. (2018). Selective basal ganglia vulnerability to energy deprivation: Experimental and clinical evidences. *Progress in Neurobiology*, *169*, 55–75. https://doi.org/10.1016/j.pneurobio.2018.07.003

Verkhratsky, A., Zorec, R., & Parpura, V. (2017). Stratification of astrocytes in healthy and diseased brain. *Brain Pathology*, *27*, 629–644. https://doi.org/10.1111/bpa.12537

Yao, Z., Gandhi, S., Burchell, V. S., Plun-Favreau, H., Wood, N. W., & Abramov, A. Y. (2011). Cell metabolism affects selective vulnerability in PINK1-associated Parkinson's disease. *Journal of Cell Science*, *124*, 4194–4202. https://doi.org/10.1242/jcs.088260

How to cite this article: Cheng X, Vinokurov AY, Zherebtsov EA, et al. Variability of mitochondrial energy balance across brain regions. *J Neurochem*. 2020;00:1–10. https://doi.org/10.1111/jnc.15239